Foundations for Gravitational Potential Energy Evaluation

Nicolas Poupart

Independent Researcher

E-mail: nicolas.poupart@yahoo.fr

Abstract. We investigate the evaluation of the effective gravitational binding energy in heterogeneous stellar systems by comparing a permutation-invariant estimator with heuristic formulations based on sequential aggregation. While the exact method provides a physically consistent reference independent of population ordering, the heuristic estimator introduces a path dependence that strongly influences the reconstructed dark-to-baryonic mass ratios.

A systematic exploration of permutations quantifies this sensitivity and shows that an optimized ordering substantially reduces the systematic bias, producing an error distribution that is approximately Gaussian and centered near zero. When applied to galactic rotation data, the heuristic approach achieves significantly higher resolution rates than the exact estimator.

These results highlight a fundamental trade-off between physical invariance and algorithmic sensitivity, and suggest that the trajectory through population space is an intrinsic component of sequential gravitational energy models.

Keywords: galaxies: kinematics and dynamics, galaxies: structure, dark matter, gravitation, methods: numerical, methods: statistical, rotation curves

Contents

1 Introduction

This article extends the previous study *"Dark Mass is Potential Energy"* [1], in which the idea of Léon Brillouin [2, 3] was developed, according to which relativistic dynamics should be renormalized by potential energy. This hypothesis, formulated prior to the observational establishment of flat galactic rotation curves [4, 5], proposed an elegant interpretation of the phenomenon. However, Brillouin did not succeed in establishing a rigorous method for renormalizing potential energy, and this natural explanation fell into oblivion because general relativity does not possess a covariant expression for gravitational energy [6] and therefore complicates the formulation of a global conservation law for gravitational energy.

The renormalization of the field $\Phi(M)$ produced by the potential energy of a set of masses M can be simply interpreted as $\Phi(\gamma M)$, in other words as if the mass M were multiplied by a renormalization factor γ. For an observer, this renormalization could be perceived as the effect of an additional baryonic mass:

$$\Phi(\gamma M) = \Phi(M) + \Phi(DM)$$

where DM would then be interpreted as invisible dark matter. This hypothesis corresponds to the current standard cosmological model [7].

In general relativity, the gravitational field is identified with the curvature of spacetime; therefore, renormalization must be understood as an increase in this curvature. Nevertheless, there exists a terminological ambiguity between 'mass', 'matter', and spacetime curvature. We often say that mass gravitates and curves spacetime, although more precisely it is energy, in all its forms, that acts as the source of curvature [8]. This curvature manifests itself as an effect commonly designated by the term "mass". Thus, if effective gravitational binding energy curves spacetime and generates an effective mass, this contribution does not necessarily act as an additional source term within the renormalized description, thereby preventing an iterative growth of the field. The extent to which gravitational binding energy may contribute to the effective mass of galaxies, however, has not yet been quantitatively established.

That this renormalization exists seems to have been numerically demonstrated by A. Deur [9–12], who argues (numerically) that the self-interaction of the gravitational field by its own energy density can produce a curvature of spacetime capable of explaining dark mass. However, these works do not make it possible to describe cosmological phenomena analytically in a simple manner. They nevertheless illustrate how gravitational binding energy generates an additional curvature that can be interpreted as an additional "mass" or as an effective renormalization of mass.

Our work uses Newtonian gravitation (NG) to calculate this field renormalization and obtain simple analytical expressions. Purists will object that this is not general relativity (GR), since we employ neither tensor mathematics nor Einstein's equations. However, it is mathematically indisputable that NG derives from GR in the weak-field approximation, and thus results derived in NG are consistent with GR in the weak-field regime. The essential advantage of this approach is that, within the Newtonian framework, effective gravitational binding energy is well defined–which makes it possible, thanks to our previous work, to deduce a correct analytical expression for the real total potential energy of a system.

However, the behavior of the evaluation of the correct energy differs from that of the heuristic we have used. We will analyze the different algorithmic alternatives for evaluating effective gravitational binding energy and their implications.

2 Exact Evaluation of the Effective Gravitational Binding Energy

We now introduce a computation scheme for effective gravitational binding energy that is both structurally linear and invariant under permutation of the constituent mass intervals. The objective is not to revisit the full theoretical construction developed previously [1], but rather to formalize a calculation procedure that preserves the physical additivity of energy while remaining independent of the ordering of stellar populations.

2.1 Linear construction of the binding energy

Consider a system decomposed into n mass intervals characterized by densities ρ_i and total masses M_i. Each interval is constructed from individual self-gravitating stars sharing the same density and is then treated as an equivalent compact sphere whose radius follows directly from mass conservation:

$$R_i = \left(\frac{3M_i}{4\pi\rho_i}\right)^{1/3} \tag{2.1}$$

The gravitational binding energy associated with this compact configuration defines a natural macroscopic energy scale:

$$\Delta E_i = \frac{3G}{5}\frac{M_i^2}{R_i} \tag{2.2}$$

Crucially, this contribution depends only on intrinsic properties of the interval and therefore enters the total energy as a strictly additive term. The system is then updated by merging this compact sphere with the previously accumulated configuration (M_c, R_c) according to volume conservation:

$$M_c \leftarrow M_c + M_i, \qquad R_c \leftarrow \left(R_c^3 + R_i^3\right)^{1/3} \tag{2.3}$$

The process is repeated sequentially for all intervals, yielding a linear accumulation of energy contributions:

$$\Delta E_{\mathrm{tot}} = \sum_{i=1}^{n} \Delta E_i + \frac{3G}{5}\frac{M_n^2}{R_n} \tag{2.4}$$

The final term represents the binding energy of the global compact configuration obtained after all mergers. In practice, it remains of the same order of magnitude as the individual interval contributions but never dominates the total energy, typically accounting for only a few percent (typically 1%-5%).

2.2 Physical and mathematical consistency of the energy estimate

The proposed evaluation of the effective gravitational binding energy is supported by three complementary arguments.

First, it follows directly from a physically grounded construction applied consistently across scales. The macroscopic energy scale GM^2/R is obtained by starting from individual stars, each treated as a self-gravitating sphere, and by aggregating them into compact configurations through volume-conserving mergers. Stellar populations are therefore not introduced as abstract blocks but emerge from the same physical logic that governs the elementary constituents. The conservative nature of the gravitational field ensures that the resulting binding energy depends only on the final configuration and not on the assembly path, while volume conservation prevents the introduction of artificial forces or unphysical density variations. The calculation thus remains firmly anchored in standard gravitational physics.

Second, the method possesses a consistent mathematical structure. The total energy is obtained through strictly additive contributions, while the final result is invariant under permutation of the mass intervals. This dual property guarantees that the estimate is independent of any arbitrary ordering of stellar populations and therefore reflects an intrinsic property of the mass distribution rather than an artifact of the algorithm.

Third, the approach demonstrates strong empirical adequacy. When applied to observed stellar populations, the resulting energy scale is empirically supported by comparisons with SPARC-based reconstructions and GALEX/SDSS photometric validations. This convergence between theoretical construction and observational constraints provides an additional indication that the estimator captures the dominant gravitational physics at galactic scales.

2.3 Algorithmic structure

Because each interval contributes through an intrinsic energy scale before being merged, the total energy depends only on the collection $\{(M_i, \rho_i)\}$ and not on the order in which the intervals are processed.

Formally, let σ be any permutation of $\{1, \ldots, n\}$. The cumulative radius after all mergers satisfies:

$$R_c^3 = \sum_{i=1}^{n} R_{\sigma(i)}^3 = \sum_{i=1}^{n} R_i^3 \tag{2.5}$$

which immediately implies that the final compact state (M_n, R_n) is unique. Since the additive contributions ΔE_i are themselves independent of ordering, the total energy remains unchanged under permutation.

This property reflects the conservative nature of the gravitational field: the binding energy is determined solely by the final mass distribution and not by the path taken to assemble it.

The resulting procedure is characterized by two essential features: (i) linearity, whereby each density class contributes an autonomous energy term, preserving the transparency of the mass–energy budget; and (ii) permutation invariance, ensuring that the final result is independent of the sequencing of stellar populations and therefore physically consistent.

Together, these properties define an exact macroscopic estimator of effective gravitational binding energy suitable for heterogeneous stellar systems.

3 Heuristic Evaluation of Effective Gravitational Binding Energy

Having established the permutation-invariant estimator, we now introduce the heuristic algorithm employed in our previous work. This procedure was preferred because it produced better empirical agreement with observations (SPARC [13]).

3.1 Algorithmic construction

Consider a stellar population described by a density ρ and total mass M, merged with an existing compact configuration (M_i, R_i). The algorithm updates the global configuration according to:

$$f(\rho, M, M_i, R_i) \to \left\{ \begin{array}{ll} M_t & = M + M_i \\ R & = \left(\dfrac{3M}{4\pi\rho}\right)^{1/3} \\ R_t & = \left(R^3 + R_i^3\right)^{1/3} \\ \Delta E_{\rm pi} & = \dfrac{3GM_t^2}{5R_t} \end{array} \right\} \to (\Delta E_{\rm pi}, M_t, R_t) \tag{3.1}$$

At each step, the incoming stellar population is first represented as an equivalent compact sphere obtained through volume conservation. The merged radius R_t then defines the characteristic gravitational scale of the updated system, from which the energy contribution is evaluated using the macroscopic form GM^2/R.

3.2 Closed-form expression as a sum

Let the n intervals be characterized by $(\rho_i, M_i)_{1 \le i \le n}$, and let $(M_0, R_0) = (0, 0)$. Define the equivalent compact radius of each interval by:

$$R_i \;=\; \left(\frac{3M_i}{4\pi\rho_i}\right)^{1/3} \tag{3.2}$$

For a chosen ordering σ of $\{1,\dots,n\}$, define the cumulative mass–radius sequence by:

$$M_j \;=\; M_{j-1} + M_{\sigma(j)}, \qquad R_j^3 \;=\; R_{j-1}^3 + R_{\sigma(j)}^3, \qquad j = 1,\dots,n \tag{3.3}$$

so that $R_j = \left(\sum_{\ell=1}^{j} R_{\sigma(\ell)}^3\right)^{1/3}$ and $M_j = \sum_{\ell=1}^{j} M_{\sigma(\ell)}$. The heuristic algorithm assigns at step j the energy:

$$\Delta E_j^{(\sigma)} \;=\; \frac{3G}{5}\,\frac{M_j^2}{R_j} \tag{3.4}$$

The heuristic total is therefore the path-dependent sum:

$$\Delta E_{\text{heur}}^{(\sigma)} \;=\; \sum_{j=1}^{n} \Delta E_j^{(\sigma)} \;=\; \frac{3G}{5} \sum_{j=1}^{n} \frac{\left(\sum_{\ell=1}^{j} M_{\sigma(\ell)}\right)^2}{\left(\sum_{\ell=1}^{j} R_{\sigma(\ell)}^3\right)^{1/3}} \tag{3.5}$$

This expression makes explicit that the heuristic estimate depends on the permutation σ through the partial sums in both mass and volume.

3.3 Interpretation

Unlike the exact linear construction introduced previously, this heuristic method evaluates the binding energy of the updated global configuration at every merger step. The procedure therefore attributes to each interval an energy that already incorporates its coupling with the previously accumulated mass.

This choice has two important consequences. First, the algorithm naturally captures the dominant gravitational scale of the system without requiring the explicit computation of intercoupling terms. Second, it introduces a path dependence: since the energy is evaluated on partially assembled configurations, the final result can vary with the ordering of the stellar populations.

This path dependence is in fact a defining strength of the heuristic estimator. The interdependence introduced at each merger step increases the sensitivity of the energy to the assembly sequence, thereby strongly constraining the space of admissible trajectories when constructing stellar populations. As a consequence, greedy optimization procedures tend to converge naturally toward a restricted set of stable solutions, whereas a fully additive formulation permits a much larger family of equivalent configurations. This controlled reduction of degeneracy makes the heuristic scheme particularly effective for recovering physically plausible stellar distributions from observational constraints.

4 Comparison of the Exact and Heuristic Estimators

We compare the permutation-invariant estimator (hereafter the *exact* method) with the heuristic algorithm within the same optimization framework applied to the SPARC dataset. For each galaxy, the algorithm searches for stellar mass distributions capable of reproducing the inferred dark mass by matching the predicted effective gravitational binding energy to the observational constraints, while enforcing the bounds $P \pm k\sigma$ on the stellar fractions. The tolerance parameter k therefore controls the accessible region of parameter space and directly impacts the solvability of the rotation-curve data.

Table 1 summarizes the fraction of resolved kinematic points and fully solved galaxies obtained with each estimator as a function of k, allowing a direct assessment of how the structural differences between the two energy formulations affect the convergence of the greedy search and the recovery of observationally consistent stellar populations.

4.1 Resolution performance

Across all tolerance levels, the heuristic estimator systematically resolves a larger fraction of both individual points and galaxies. The difference is modest at 1σ, where both methods operate under strong constraints, but becomes pronounced as the admissible parameter space expands.

At 2σ, the contrast is already significant: the heuristic method nearly doubles the number of solved galaxies when the second distribution is included. The effect becomes decisive at 3σ, where the heuristic algorithm approaches full resolution of the dataset, exceeding 99% of solved points and more than 93% of galaxies, while the exact estimator remains close to the 50% level.

4.2 Origin of the performance gap

This discrepancy follows directly from the structural differences between the two estimators. The exact formulation is strictly additive and permutation-invariant, which implies that many stellar configurations produce comparable energy levels. While mathematically consistent, this enlarged degeneracy weakens the sensitivity of the optimization process and makes convergence toward observationally compatible populations more difficult.

By contrast, the heuristic estimator introduces controlled path dependence. Because each merger step modifies the global gravitational scale, the admissible trajectories through parameter space become strongly constrained. This increased sensitivity acts as an implicit regularization mechanism for greedy optimization procedures, guiding them toward a restricted subset of stable solutions.

Table 1. Comparison of resolution as a function of the k-factor and method used

	First Distribution		With Second Distribution	
k **method**	**Points Solved**	**Galaxies Solved**	**Points Solved**	**Galaxies Solved**
1σ Exact	746 (24.5%)	18 (10.3%)	809 (26.5%)	25 (14.4%)
1σ Heuristic	790 (25.9%)	22 (12.6%)	1082 (35.5%)	29 (16.7%)
2σ Exact	1207 (39.6%)	59 (33.9%)	1309 (43.0%)	67 (38.5%)
2σ Heuristic	1372 (45.0%)	82 (47.1%)	3010 (98.8%)	158 (90.8%)
3σ Exact	1560 (51.2%)	93 (53.4%)	1514 (49.7%)	93 (53.4%)
3σ Heuristic	1930 (63.3%)	107 (61.5%)	3022 (99.1%)	162 (93.1%)

4.3 Photometric validation: GALEX and SDSS correlations

Beyond the purely dynamical resolution rates reported in Table 1, the two estimators can be compared through an independent photometric validation. For each reconstructed stellar population, we compute synthetic ultraviolet and optical colors and test their correspondence with GALEX and SDSS observations [14–18] using Pearson and Spearman correlation analyses.

Table 2 summarizes the predicted–observed correlations obtained with the exact and heuristic estimators for four color indices. The comparison is performed in identical conditions (same galaxy sets and same statistical procedures), so that differences can be attributed to the structure of the energy estimator and its impact on the recovered stellar populations.

Table 2. Correlation analysis between predicted and observed galaxy colors. Pearson r and Spearman ρ coefficients are reported together with their Gaussian-equivalent significances. Linear fits are reported in rank–rank space.

Color	N	$r_{\rm P}$	$\sigma_{\rm P}$	$\rho_{\rm S}$	$\sigma_{\rm S}$	$b_{\rm rank} \pm 1\sigma$
$g-r$ Exact	128	0.430	5.34	0.490	6.30	0.490 ± 0.078
$g-r$ Heuristic	128	0.483	6.19	0.611	8.66	0.611 ± 0.071
NUV–r Exact	119	0.461	5.62	0.546	7.04	0.546 ± 0.077
NUV–r Heuristic	119	0.522	6.63	0.586	7.83	0.586 ± 0.075
$r-z$ Exact	129	0.212	2.45	0.430	5.36	0.430 ± 0.080
$r-z$ Heuristic	129	0.325	3.88	0.393	4.81	0.393 ± 0.082
FUV–NUV Exact	136	-0.152	1.78	-0.263	3.16	-0.263 ± 0.083
FUV–NUV Heuristic	136	-0.049	0.57	-0.313	3.82	-0.313 ± 0.082

Overall, both methods produce statistically significant ordering relations across multiple bands, confirming that dynamical constraints alone can generate structured stellar population mixtures. However, the relative performance depends on the wavelength range and on whether linear or rank-based correlations are considered.

For the optical $g-r$ color, the heuristic estimator yields the strongest monotonic ordering, with a Spearman coefficient $\rho_{\rm S} = 0.611$ (8.66σ), compared to $\rho_{\rm S} = 0.490$ (6.30σ) for the exact method. A similar improvement is observed for the mixed UV–optical color NUV–r, where the heuristic approach increases both Pearson and Spearman correlations. These two indices are the most sensitive to the global population balance between low-mass main-sequence stars and denser components, and the heuristic path dependence appears to provide the additional selectivity required for robust cross-galaxy ordering.

For the $r-z$ optical color, the situation is inverted: the exact estimator provides a slightly stronger rank correlation $\rho_{\rm S} = 0.430$ (5.36σ) than the heuristic method $\rho_{\rm S} = 0.393$ (4.81σ), corresponding to a significance ratio of ~ 1.1 (Gaussian-equivalent), while the heuristic improves the Pearson coefficient. This indicates that both reconstructions encode a meaningful optical ordering, but with different trade-offs between monotonic ranking and linear coherence in raw color space.

Finally, the purely ultraviolet color FUV–NUV remains the least monotonic indicator for both methods. Both estimators produce only moderate anticorrelations, with the heuristic method exhibiting a weaker Pearson coefficient but a stronger Spearman coefficient. This behavior is consistent with the known multi-regime structure of ultraviolet colors, where distinct star-formation histories can overlap in integrated UV indices and naturally weaken global monotonic trends.

Taken together, these results show that the heuristic estimator tends to enhance the recoverability of population ordering from dynamics, particularly in $g-r$ and NUV–r, while the exact estimator can remain competitive in specific optical bands. This reinforces the interpretation advanced above: the permutation-invariant estimator provides a structurally rigorous energy scale, whereas the heuristic estimator introduces a controlled dependence that acts as an effective constraint on the reconstruction and can improve convergence toward observationally consistent stellar population orderings.

4.4 Interpretation

The comparison highlights a fundamental trade-off between mathematical invariance and algorithmic efficiency. The exact estimator provides a structurally rigorous definition of the gravitational binding energy, whereas the heuristic method behaves as a powerful inference operator capable of rapidly identifying stellar populations consistent with observational constraints.

In practice, the strong empirical performance of the heuristic approach suggests that the induced trajectory constraint captures relevant physical structure within the stellar distribution. Rather than being a drawback, the path dependence appears to supply the level of selectivity required for large-scale galactic reconstruction.

5 Analysis of the Sensitivity of the Heuristic

The reconstruction begins from a reference stellar population spanning a wide range of intrinsic densities, from diffuse main-sequence stars to ultra-compact remnants. The components include black holes (BH), neutron stars (NS), white dwarfs (WD), red giants (RG), and the standard spectral classes from O to M. This basis is not intended to reproduce a detailed stellar census; rather, it provides a physically motivated density spectrum capable of generating the gravitational energy required by the dynamical constraints. Since the energy response is strongly non-linear with respect to density, different permutations of the same components can lead to distinct reconstruction trajectories, making the ordering itself an object of study rather than an imposed assumption.

For nearby galaxies ($z \approx 0$), consistent with the populations represented in SPARC, we adopt average mass fractions normalized to unity:

$$\begin{array}{lll} \mathrm{BH} = 1.0\% \pm 0.5\% & \mathrm{NS} = 0.3\% \pm 0.1\% & \mathrm{WD} = 2.2\% \pm 0.7\% \\ \mathrm{RG} = 0.2\% \pm 0.1\% & \mathrm{M} = 55\% \pm 10\% & \mathrm{K} = 16\% \pm 6\% \\ \mathrm{G} = 10.5\% \pm 5\% & \mathrm{F} = 5.5\% \pm 3\% & \mathrm{A} = 5\% \pm 2\% \\ \mathrm{B} = 3\% \pm 1\% & \mathrm{O} = 1.3\% \pm 0.5\% & \end{array}$$

These fractions reflect the well-established dominance of low-mass stars in the stellar mass budget, while compact remnants provide a small but dynamically significant contribution. The ordered list [BH, NS, WD, RG, M, K, G, F, A, B, O] will hereafter be referred to as the original (or initial) ordering, as it corresponds to the sequence adopted in our previous work.

5.1 Permutation analysis

Figure 1 displays the ratio DM/M_{bar} produced by 1×10^5 different permutations of the stellar population ordering. A broad fluctuation band is observed, spanning from a minimum ratio of 0.8 to a maximum of 128, illustrating the strong dependence of the heuristic estimator on the chosen population sequence.

The permutation corresponding to strictly increasing density yields an exceptionally large ratio of 120.5, whereas the strictly decreasing density ordering produces a much lower value of 1.9. The original ordering adopted in our previous work yields 50.2, whereas the exact value is 55.6 for all permutations, corresponding to an error of approximately 10%.

Across all permutations, the median ratio is 12, while the mean reaches 21.4, revealing a strongly skewed distribution with a long high-ratio tail that significantly shifts the mean.

Overall, this figure highlights the pronounced sensitivity of the heuristic estimator to the ordering of stellar populations.

Figure 1. Distribution of the predicted dark-to-baryonic mass ratio across 1×10^5 stellar population permutations. Each bin groups the permutations yielding ratios within the corresponding range, highlighting the strong sensitivity of the heuristic estimator to population ordering.

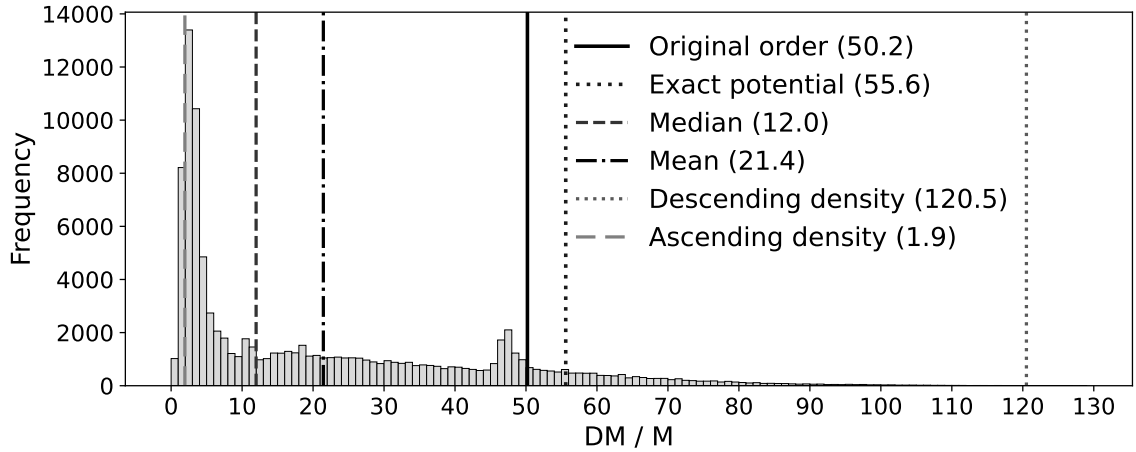

5.2 Proportion analysis

Figure 2 shows the relative error in the dark-to-baryonic mass ratio obtained with the heuristic estimator compared to the exact method for the original permutation. The histogram is generated from 1×10^5 distinct stellar fractions satisfying the 1σ constraint.

The error spans approximately from -20% to -5%, revealing a systematic bias in the heuristic prediction. Applying a rescaling factor of 1.1 to the dark mass computed with the heuristic estimator reduces this offset and shifts the error interval to roughly -10% to 5%. After this adjustment, the distribution becomes nearly centered, with a mean relative error of -1.2% and a median of -0.6%.

Figure 3 shows the error histogram obtained for the permutation [NS, A, WD, B, K, BH, M, RG, G, F, O], identified through a greedy search starting from the original ordering. The improvement is immediately visible: a simple scaling by 1.01 is sufficient to center the distribution on zero.

The resulting error closely follows a Gaussian profile, spanning approximately from -5% to 5%, which indicates that the systematic bias observed for the original permutation has effectively disappeared.

5.3 Comparison of the old and new heuristic estimators

Tables 3 and 4 compare the performance of the exact estimator with two heuristic implementations that differ solely by the ordering of the stellar populations. The underlying algorithm, physical assumptions, and parameter space are strictly identical; only the permutation is modified.

Table 3 shows that both heuristic variants significantly outperform the exact estimator in terms of resolved kinematic points and solved galaxies. The old heuristic achieves the highest resolution rates, particularly when the second distribution is included, solving nearly

Figure 2. Distribution of the relative error in the dark-to-baryonic mass ratio between the heuristic and exact estimators for the original permutation under the 1σ constraint, computed from 1×10^5 stellar fraction realizations. The thick black line indicates the median of the distribution, while the dashed lines mark the $\pm 1\sigma$, $\pm 2\sigma$, and $\pm 3\sigma$ intervals.

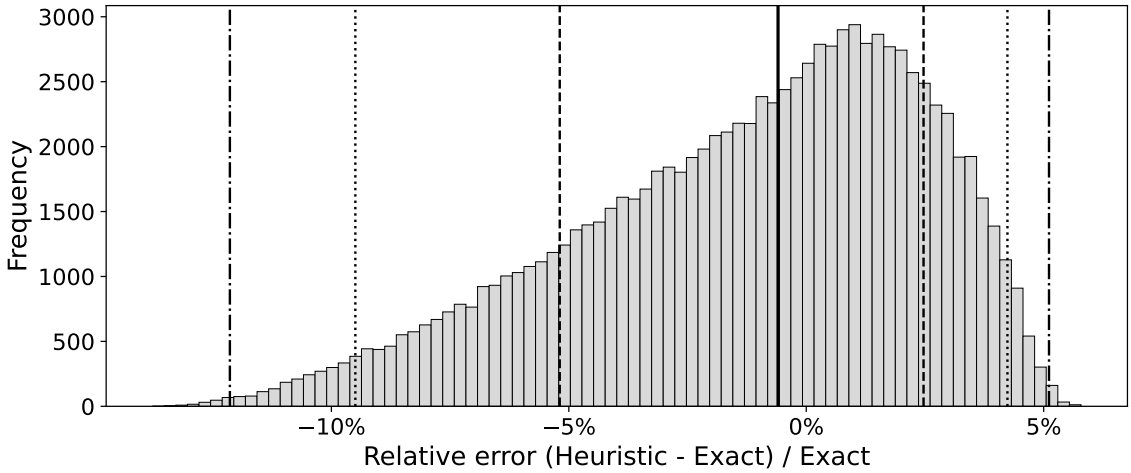

Figure 3. Distribution of the relative error in the dark-to-baryonic mass ratio between the heuristic and exact estimators for the permutation [NS, A, WD, B, K, BH, M, RG, G, F, O] under the 1σ constraint, computed from 1×10^5 stellar fraction realizations. The thick black line indicates the median of the distribution, while the dashed lines mark the $\pm 1\sigma$, $\pm 2\sigma$, and $\pm 3\sigma$ intervals.

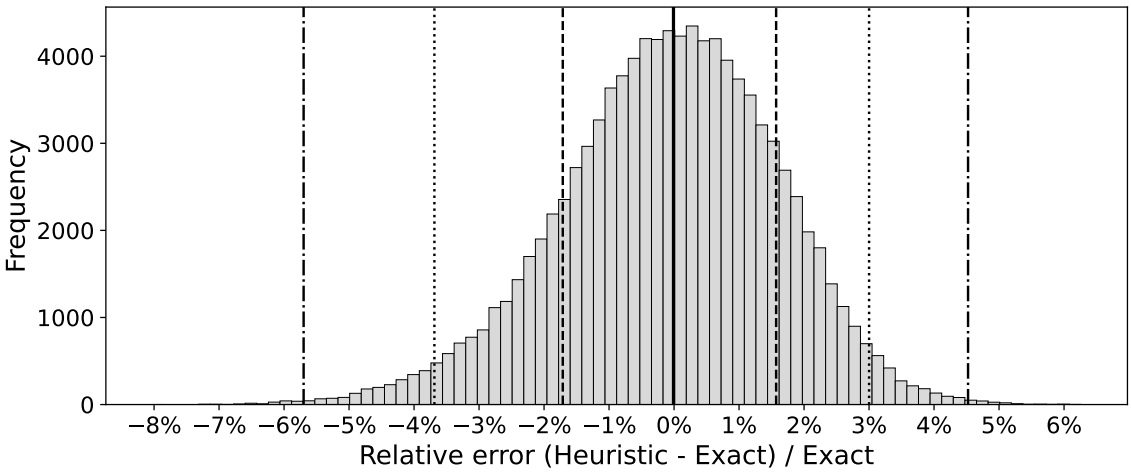

all data points at 2σ. The new heuristic remains very close to this performance, with only a modest reduction in convergence efficiency.

Because the algorithm itself is unchanged, these differences directly quantify the impact of population ordering on the heuristic reconstruction. The results therefore provide empirical evidence of the strong path dependence introduced by the sequential structure of the estimator.

Table 4 further evaluates the statistical consistency of the reconstructed populations

through correlations between predicted and observed galaxy colors. For the optical $g - r$ and mixed NUV–r indices, both permutations produce strong and highly significant monotonic relations, well above those obtained with the exact estimator. The new permutation slightly reduces the Pearson coefficients while preserving comparable Spearman correlations, indicating that the global ordering of galaxies remains largely intact.

For the $r - z$ color, the exact estimator retains the strongest rank correlation, whereas both heuristic permutations yield weaker but still significant trends. The most pronounced change occurs in the FUV–NUV index, where the new permutation produces a positive correlation instead of the moderate anticorrelation obtained previously. Since the algorithm is otherwise identical, this shift demonstrates that ultraviolet ordering is particularly sensitive to the sequence in which stellar components are aggregated.

Taken together, these results show that permutation alone can measurably affect both convergence efficiency and photometric ordering. The heuristic estimator is therefore not defined solely by its mathematical form, but also by the trajectory it follows through population space, suggesting that the reconstruction path itself constitutes an intrinsic component of sequential gravitational energy models.

Table 3. Comparison of resolution as a function of the k-factor and method used

	First Distribution		**With Second Distribution**	
k **method**	**Points Solved**	**Galaxies Solved**	**Points Solved**	**Galaxies Solved**
1σ Exact	746 (24.5%)	18 (10.3%)	809 (26.5%)	25 (14.4%)
1σ Old	790 (25.9%)	22 (12.6%)	1082 (35.5%)	29 (16.7%)
1σ New	750 (24.6%)	18 (10.3%)	965 (31.7%)	27 (15.5%)
2σ Exact	1207 (39.6%)	59 (33.9%)	1309 (43.0%)	67 (38.5%)
2σ Old	1372 (45.0%)	82 (47.1%)	3010 (98.8%)	158 (90.8%)
2σ New	1240 (40.7%)	67 (38.5%)	2980 (97.8%)	148 (85.1%)
3σ Exact	1560 (51.2%)	93 (53.4%)	1514 (49.7%)	93 (53.4%)
3σ Old	1930 (63.3%)	107 (61.5%)	3022 (99.1%)	162 (93.1%)
3σ New	1614 (53.0%)	102 (58.6%)	3014 (98.9%)	163 (93.7%)

6 Conclusion

In this work, we have examined the evaluation of effective gravitational binding energy in heterogeneous stellar systems by comparing a permutation-invariant estimator with heuristic formulations based on sequential aggregation. The exact estimator provides a physically grounded reference framework: its linear structure ensures a transparent energy budget, while permutation invariance guarantees that the result depends only on the final configuration of the system.

By contrast, the heuristic estimator introduces a controlled path dependence through the ordering of stellar populations. The analysis shows that this ordering alone can significantly affect both convergence efficiency and the reconstructed dark-to-baryonic mass ratios. A systematic exploration of permutations reveals a wide dispersion of outcomes, thereby quantifying the intrinsic sensitivity of the heuristic approach.

Despite this sensitivity, the heuristic method demonstrates strong practical performance when applied to galactic rotation data. In particular, an optimized permutation substantially

Table 4. Correlation analysis between predicted and observed galaxy colors. Pearson r and Spearman ρ coefficients are reported together with their Gaussian-equivalent significances. Linear fits are reported in rank–rank space.

Color	N	r_{P}	σ_{P}	ρ_{S}	σ_{S}	$b_{\mathrm{rank}} \pm 1\sigma$
$g-r$ Exact	128	0.430	5.34	0.490	6.30	0.490 ± 0.078
$g-r$ Old	128	0.483	6.19	0.611	8.66	0.611 ± 0.071
$g-r$ New	128	0.221	2.55	0.587	8.14	0.587 ± 0.072
NUV–r Exact	119	0.461	5.62	0.546	7.04	0.546 ± 0.077
NUV–r Old	119	0.522	6.63	0.586	7.83	0.586 ± 0.075
NUV–r New	119	0.396	4.66	0.598	8.06	0.598 ± 0.074
$r-z$ Exact	129	0.212	2.45	0.430	5.36	0.430 ± 0.080
$r-z$ Old	129	0.325	3.88	0.393	4.81	0.393 ± 0.082
$r-z$ New	129	-0.045	0.51	0.358	4.33	0.358 ± 0.083
FUV–NUV Exact	136	-0.152	1.78	-0.263	3.16	-0.263 ± 0.083
FUV–NUV Old	136	-0.049	0.57	-0.313	3.82	-0.313 ± 0.082
FUV–NUV New	136	0.318	3.88	0.433	5.56	0.433 ± 0.078

reduces the systematic bias observed in the original ordering while preserving high resolution rates across the SPARC sample. The resulting error distribution becomes nearly Gaussian and centered on zero after a minimal rescaling, indicating that the estimator remains statistically well behaved.

Correlation analyses between predicted and observed galaxy colors further confirm that the reconstructed stellar populations retain a meaningful cross-galaxy ordering. Although the exact estimator offers stronger guarantees of physical consistency, the heuristic formulations exploit their sequential structure to enhance selectivity within the population space. The comparison therefore highlights a fundamental trade-off between physical invariance and algorithmic sensitivity.

Taken together, these results suggest that effective gravitational binding energy can be robustly evaluated at macroscopic scales while remaining sensitive to the internal organization of stellar populations. The exact estimator establishes the physical baseline, whereas optimized heuristic orderings provide an efficient pathway toward realistic galactic reconstructions.

More broadly, the present analysis emphasizes that, in sequential energy formulations, the trajectory through population space constitutes an intrinsic component of the model. Understanding and controlling this trajectory appears essential for reconciling computational efficiency with physical interpretability in large-scale gravitational systems.

Whether this trajectory reflects an underlying physical constraint or an emergent property of the reconstruction procedure remains an open question. The stability observed across optimized configurations nevertheless suggests that realistic stellar populations may occupy a naturally restricted region of parameter space.

Software availability

The C++ program used to perform all numerical calculations and generate the corresponding graphs are freely available at dark-mass-generator.sourceforge.io or at doi.org/10.6084/m9.figshare.30543527.

Funding

This research received no specific grant from any funding agency in the public, commercial, or not-for-profit sectors.

Competing interests

The author declares no competing interests.

Roles

The author conceived the study, performed the analysis, and wrote the manuscript.

References

[1] N. Poupart, "Dark mass is potential energy." Preprint available at FigShare (doi.org/10.6084/m9.figshare.30543407) and ResearchGate (doi.org/10.13140/RG.2.2.15355.43046), 2025.

[2] L. Brillouin, *L'enigme $E = Mc^2$: Energie potentielle et renormalisation de la masse*, *Journal de Physique* **25** (1964) .

[3] L. Brillouin, *The mass of a system of potential energy*, *Proceedings of the National Academy of Sciences of the United States of America* **53** (1965) .

[4] V.C. Rubin, J. Ford, W. Kent and N. Thonnard, *Rotational properties of 21 sc galaxies with a large range of luminosities and radii, from ngc 4605 (r = 4kpc) to ugc 2885 (r = 122kpc)*, *The Astrophysical Journal* **238** (1980) 471.

[5] A. Bosma, *The distribution and kinematics of neutral hydrogen in spiral galaxies of various morphological types*, Ph.D. thesis, Rijksuniversiteit Groningen, 1978.

[6] C.W. Misner, K.S. Thorne and J.A. Wheeler, *Gravitation*, W. H. Freeman (1973).

[7] T. Clifton, P.G. Ferreira, A. Padilla and C. Skordis, *Modified gravity and cosmology*, *Physics Reports* **513** (2012) 1.

[8] R.C. Tolman, *Relativity, Thermodynamics and Cosmology*, Oxford University Press (1934).

[9] A. Deur, *An explanation for dark matter and dark energy consistent with the standard model of particle physics and general relativity*, *European Physical Journal C* **79** (2019) 883.

[10] A. Deur, C. Sargent and B. Terzic, *Significance of gravitational nonlinearities on the dynamics of disk galaxies*, *The Astrophysical Journal* **896** (2020) 94.

[11] A. Deur, *Relativistic corrections to the rotation curves of disk galaxies*, *European Physical Journal C* **81** (2021) 213.

[12] A. Deur, *Effect of the field self-interaction of general relativity on the cosmic microwave background anisotropies*, *Classical and Quantum Gravity* **39** (2022) 135003.

[13] F. Lelli, S.S. McGaugh and J.M. Schombert, *Sparc: Mass models for 175 disk galaxies with spitzer photometry and accurate rotation curves*, *The Astronomical Journal* **152** (2016) 157.

[14] N. Poupart, "Stellar population ordering from galactic dynamics." Preprint available at FigShare (doi.org/10.6084/m9.figshare.31175302) and ResearchGate (doi.org/10.13140/RG.2.2.35654.74561), 2026.

[15] D.C. Martin et al., *The galaxy evolution explorer: A space ultraviolet survey mission*, *The Astrophysical Journal Letters* **619** (2005) L1.

[16] L. Bianchi et al., "Galex gr5 x sdss dr7 matched catalogs." MAST / STScI High-Level Science Products, 2011.

[17] D.G. York et al., *The sloan digital sky survey: Technical summary*, *The Astronomical Journal* **120** (2000) 1579.

[18] M. Fukugita, T. Ichikawa, J.E. Gunn, M. Doi, K. Shimasaku and D.P. Schneider, *The sloan digital sky survey photometric system*, *The Astronomical Journal* **111** (1996) 1748.